

Static test on failure process of tubular T-joints with initial fatigue crack

Yamin Wang¹, Yongbo Shao^{*1}, Shengzhi Song² and Dongping Yang³

¹ School of Mechatronic Engineering, Southwest Petroleum University, Chengdu 610500, P.R. China

² R&D centre of Jungian Construction safety and disaster mitigation, Jiangsu Jianzhu Institute, Xuzhou 221116, P.R. China

³ Technology Inspection Center, China Petroleum & Chemical Corporation, Dong 257062, P.R. China

(Received December 24, 2016, Revised May 04, 2017, Accepted May 17, 2017)

Abstract. Fatigue crack initiated in welded tubular joints due to cyclic loading may produce harmful effect on the integrity of the tubular structures. To study such effect, both fatigue and static tests on nine circular tubular T-joint specimens made of carbon steel materials were carried out. The specimens were subjected to tensile loading in both fatigue and static tests. The load-displacement relation, the crack propagation and the failure mode of the specimens are all analyzed. The deterioration of the static strength of the cracked T-joints is also investigated and evaluated through an area reduction factor. Experimental results indicate that the static strength of a tubular T-joint with a surface crack seems to decrease slightly while a through crack has relatively remarkable effect on the reduction of the static strength. Additionally, experimental results also show that the toughness of the materials and the geometry of the specimens play an important role on the failure process of cracked tubular T-joints.

Keywords: tubular T-joints; fatigue crack; residual static strength; failure mode; experimental test

1. Introduction

Welded tubular structures are very common in offshore jacket platforms. In these structures, steel tubes with circular hollow section are connected together through penetration weld to form a tubular joint. Both high stress concentration and welding residual stresses exist along the weld toe in a tubular joint to cause the region around the weld toe to be much brittle. Investigation on stress concentration at the weld toe in a tubular joint has been carried out for decades, and some reports in this field were still found recently (Liu *et al.* 2016, Yang *et al.* 2016). When a tubular joint is subjected to cyclic loading produced by wind and seawater wave, fatigue crack occurs after some loading cycles. Many studies in the fatigue assessment of welded tubular joints in the literature based on experimental tests and corresponding theoretical methods were reported (Chiew *et al.* 2004, 2009, Shao and Cao 2005, Fathi and Aghakouchak 2007, Mashiri and Zhao 2010, Hanji *et al.* 2014, Jia *et al.* 2016). Some researchers (Lee *et al.* 2005, Borges *et al.* 2012, Shen and Choo 2012, Jiki and Agber 2014, Liu *et al.* 2016, Yagi *et al.* 2017) presented numerical simulation on cracked tubular joints by using FEM or BEM. Jia (2014) investigated the effect of post weld treatment on cracking of beam-column connections, and it was found that the fatigue behavior of beam-column connections was improved efficiently after post weld treatment. Thandavamoorthy (2004) evaluated the reserve capacity of fatigue damaged internally ring stiffened tubular joints, and

an analytical method was given for assessing such reserve capacity.

For a tubular joint containing a fatigue crack, some static tests were carried out to investigate its failure process. Zerbst *et al.* (2002) studied the fracture behavior of a welded tubular T-joint with a surface crack at the weld toe through static test. It aims to provide a reliable and accurate assessment on the integrity of cracked tubular joints. The experimental result shows a plastic rather than brittle failure occurs for the specimen. However, this work cannot provide regularity of conclusions because only one specimen was tested. A detailed study on the residual static strength of high strength steel tubular joints with fatigue crack was conducted by Talei-Faz *et al.* (2004). It was found that the load carrying capacity of the high strength steel tubular joints was not severely hampered by relatively large cracked sections. However, this study still recommends to conduct a larger number of tests so as to establish a more definitive pattern.

Although the above research studies on the static strength of cracked tubular joints were conducted, there are still some insufficiency in them. In the research work reported by Zerbst *et al.* (2002), the geometry of the tested specimens was same although the crack sizes in the specimens were different. In the reported study by Talei-Faz *et al.* (2004), the specimens in the experimental test were made of high strength material. However, carbon steel is more commonly used in the offshore jacket platforms. Lie *et al.* (Lie and Yang 2009a, b, Lie *et al.* 2009) then carried out both experimental test and numerical simulation to evaluate the fracture failure of square tubular joints. In their experimental tests, the cracks of all the specimens were produced from fatigue test. Bjork *et al.* (2008) assessed the subzero fracture of welded square tubular K-joint at

*Corresponding author, Professor,
E-mail: cybshao2009@hotmail.com

different low temperatures, and it was found that initial ductile tearing led to brittle failure at low temperatures. However, tubular joints with circular hollow section rather than square hollow section are more widely used in offshore jacket platforms. The static behavior of concrete-filled circular tubular joints with initial fatigue crack was also investigated through experimental test (Cui and Shao 2015). Qian and Li (2013) presented approach for assessing the resistance of cracked steel plates. Thereafter, they evaluated the static behavior of tubular joints based on elastic-plastic energy release rate and material fracture resistance respectively (Qian *et al.* 2013, Zhang and Qian 2013).

Based on the above considerations, this study aims to investigate the effect of fatigue crack on the static failure of circular tubular joints under tension. The tested tubular joints are made of carbon steel materials and the cracks in

these tubular joints are produced from fatigue tests of the tubular T-joints under tensile loading cycles.

2. Setup and preparation of experimental test

2.1 Specimens

The specimens in the experimental tests are circular hollow section tubular T-joints. A typical circular tubular T-joint is shown in Fig. 1. A brace member is welded onto the outer surface of a chord member by using penetration weld. After welding, the weld quality is checked through ultrasonic technique to ensure that there is no initial defect such as crack along the weld toe. Some normalized parameters, which are generally used to denote the geometry of a tubular joint such as β , γ , τ and α , are also defined in Fig. 1. Overall three groups of specimens are designed as tabulated in Table 1. In each group, four specimens with same dimensions are fabricated. One of them is used to study the static strength without crack, and the other three specimens are designed to experience fatigue test firstly to produce fatigue crack at the weld toe. Then, the three specimens are tested statically to study the failure process and the fracture behavior. From the comparison between static performance of both the un-cracked and the cracked specimens, the deterioration of the static strength of the cracked tubular T-joints can be evaluated.

The steel materials used in the steel tubes are all Q235B which is a steel material widely used in China. After fabri-

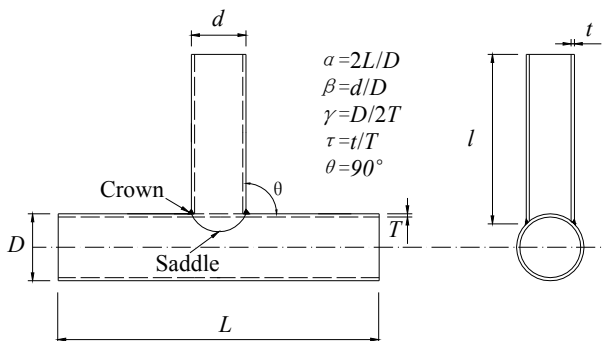


Fig. 1 A typical circular tubular T-joint

Table 1 Geometrical parameters of T-joint specimens

Group	Specimen	D (mm)	T (mm)	L (mm)	l (mm)	β	γ	τ
CTJ180	CTJ180-1	180	8	2000	400	0.739	11.25	0.75
	CTJ180-2	180	8	2000	400	0.739	11.25	0.75
	CTJ180-3	180	8	2000	400	0.739	11.25	0.75
	CTJ180-4	180	8	2000	400	0.739	11.25	0.75
CTJ219	CTJ219A-1	219	6	2000	400	0.493	18.25	1
	CTJ219A-2	219	6	2000	400	0.493	18.25	1
	CTJ219B-1	219	6	2000	400	0.493	18.25	1
	CTJ219B-2	219	6	2000	400	0.493	18.25	1
CTJ159	CTJ159A-1	159	8	2000	300	0.28	9.9	0.75
	CTJ159B-1	159	8	2000	300	0.28	9.9	0.75
	CTJ159B-2	159	8	2000	300	0.28	9.9	0.75
	CTJ159B-3	159	8	2000	300	0.28	9.9	0.75

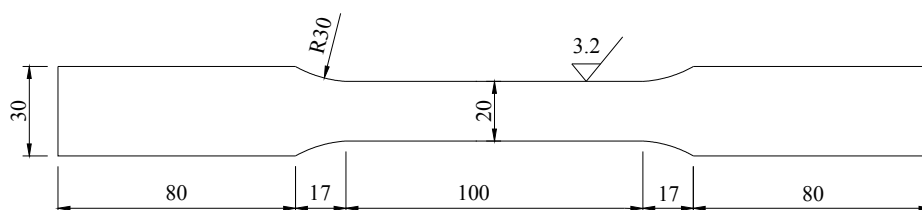


Fig. 2 Coupon test specimens (dimensions in mm)

Table 2 Material properties (steel Q235B)

Specimen	Yield strength (MPa)	Tensile strength (MPa)	Elongation (%)
CTJ180	389.5	591.9	24.5
CTJ219A	322.0	594.3	25.0
CTJ219B	290.2	585.5	25.5
CTJ159A	349.1	626.2	28.0
CTJ159B	321.0	669.8	30.5

cation of the specimens, the material properties of the braces and the chords are measured from uni-axial tensile tests for the coupons as shown in Fig. 2. The yield strength, the tensile strength and the elongation percentage of the steel materials are listed in Table 2. It should be noted that the specimens in the group CTJ219 and CTJ159 are classified into two types based on their slightly different material properties from experimental measurements.

2.2 Test rig

Both fatigue and static tests are carried out in the test rig as shown in Fig. 3. The chord is hinged at its both ends by connecting to the supports with pins. Axial load is applied to the brace end of the T-joint through the test rig with a loading magnitude of 500 kN and a maximum displacement of 75 mm. The maximum frequency in the sinusoidal cyclic loading that the test rig can produce is 20 Hz. During the test, the applied axial load as well as the displacement at the brace end is recorded automatically from the data acquisition system.

2.3 Hot spot stress measurement

In the fatigue test, the location of the crack is determined by the peak stress around the weld toe. The stress along the weld toe is generally called hot spot stress, which is very important in evaluating the fatigue life of welded tubular structures, and its distribution along the weld toe is mainly influenced by the joint’s geometry, such as the values of parameters γ and β . It has been investigated that the peak hot spot stress may be located at different positions when the geometry of a tubular T-joint is changing (Shao 2007).

In the definition on the hot spot stress around the weld

toe, the stress component perpendicular to the weld is at present accepted by many design guidelines such as IIW (1999) and CIDCET (Wardenier *et al.* 2008). This definition is widely used in the fatigue design for welded tubular structures. To monitor the crack development, the location of the peak hot spot stress is necessary to be determined before the fatigue test. As all of the four specimens in each group as listed in Table 1 have the same geometry, the hot spot stress distribution is assumed reasonably to be almost same although the difference of the weld size may produce slight influence on such stress distribution. Therefore, one specimen in each group is selected to measure the hot spot stress distribution before fatigue test.

It is well known that the stress is generally calculated from the strain measured from strain gauge placed on the specimen. However, the strain gauge cannot be placed directly at the weld toe because the weld surface and the chord surface are not located in a same plane. To overcome this problem, the strain gauge can be arranged in a region close to the weld toe, and this region is called “extrapolation region” as shown in Fig. 4. The extrapolation region is determined by the geometry of the tubular joint. In CIDCET (Wardenier *et al.* 2008), the specified extrapolation region for a circular tubular joint is listed in Table 3. R and r in Table 3 are the radii of the chord and the brace respectively. For a circular tubular joint, CIDCET (Wardenier *et al.* 2008) recommends to calculate the hot spot stress at the weld toe by using linear extrapolation method, i.e., two strain gauges perpendicular to the weld toe can be placed in the extrapolation region. Huang (2002) verified the accuracy of the linear extrapolation method for

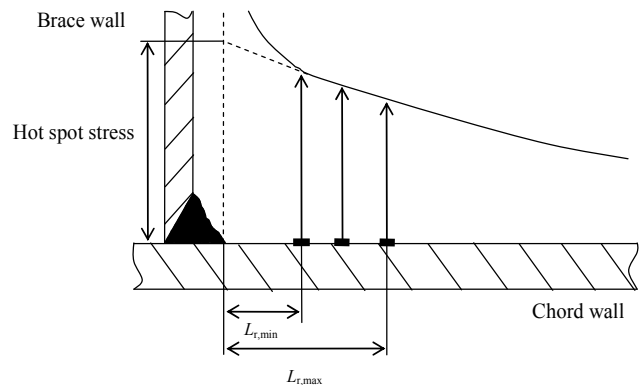
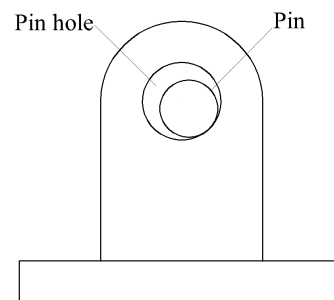


Fig. 4 Extrapolation region



(a) View of tested specimen



(b) Pinned connection at support

Fig. 3 Test rig

Table 3 Extrapolation region for circular tubular joints

From weld toe	Chord		Brace	
	Saddle	Crown	Saddle	Crown
$L_{r,min}$ *	$0.4T$	$0.4T$	$0.4t$	$0.4t$
$L_{r,max}$ **	$0.09R$	$0.4\sqrt{RTrt}$	$0.65\sqrt{rt}$	$0.65\sqrt{rt}$

Note: *Minimum value of $L_{r,min}$ is 4 mm

** Maximum value of $L_{r,max}$ is $L_{r,min}+0.6t$

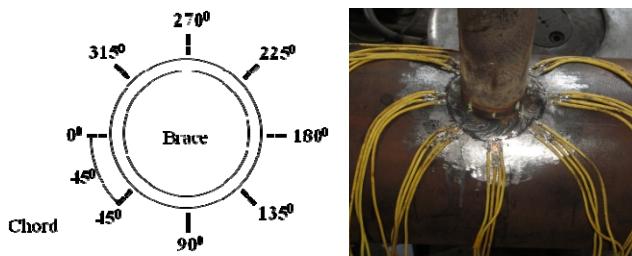


Fig. 5 Placement of strain gauges

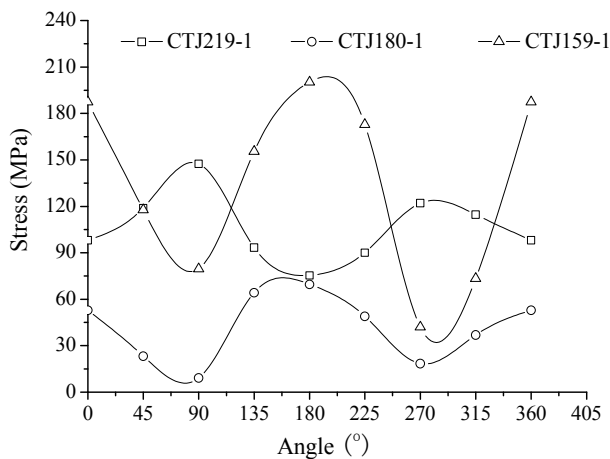


Fig. 6 Hot spot stress distribution around weld toe

measuring the hot spot stress around the weld toe for circular tubular T-joints through finite element investigation.

For each specimen, eight locations with an interval of 45° around the weld toe are selected to place strain gauges in the extrapolation region as shown in Fig. 5. Before

fatigue tests, an axial tension of 20 MPa is applied at the brace end of each specimen, and the hot spot stress distribution around the weld toe is calculated from the measured strain values, and the result is shown in Fig. 6. The detailed method for calculating the hot spot stress around the weld toe from the measured strains in the extrapolation region was introduced by Shao (2005). The location of 0° in Fig. 6 is the crown and 90° refers to a position located at the saddle. Obviously, 180° and 270° are the other crown and the other saddle positions respectively. The maximum and the minimum magnitudes in the cyclic loading for each specimen, together with the loading frequency, are summarized in Table 4.

The tested results show that the maximum hot spot stresses for the specimens in the groups of CTJ159 and CTJ180 are all located at 180° while such position for specimens in the group of CTJ219 is located at 90° . The above results indicate that the fatigue cracks for the specimens in the groups of CTJ159 and CTJ180 are expected to initiate at the crown while the saddle is the expected initiation position of the fatigue cracks for the specimens in the group of CTJ219. It is noted here that the location of the peak stress at the weld toe of a tubular T-joint was proved to be possibly located at crown or saddle based on the joint's geometry (Shao 2007) although previous static tests on cracked tubular T-joints were all assumed that the fatigue crack was located at the saddle position.

3. Fatigue test and results

In the groups of CTJ180 and CTJ159 listed in Table 1, three specimens in each group are selected for carrying out both fatigue and static tests. The remaining one in each group is used to conduct only static test for comparing the difference in static strength. In the group of CTJ219, specimens CTJ219A-1, CTJ219A-2 and CTJ219B-1 are selected for conducting fatigue and static tests while specimen CTJ219-B2 is selected for conducting only static test. All the fatigue tests are conducted by using the instrument as shown in Fig. 3(a). The average value, the amplitude and the frequency of the cyclic loading, as well as the loading cycles, can be monitored and recorded simultaneously during the fatigue tests.

The cyclic loading in the fatigue tests is sinusoidal as

Table 4 Results of fatigue test

Specimen	Max. load (kN)	Min. load (kN)	Frequency (HZ)	Loading cycle ($\times 10^4$)	Crack location
CTJ180-1	125	30	3.0	2.60	Crown
CTJ180-2	97	10	3.0	19.46	Crown
CTJ180-3	97	10	3.0	20.03	Crown
CTJ219A-1	40	10	3.0	19.29	Saddle
CTJ219A-2	40	10	3.0	20.70	Saddle
CTJ219B-1	40	10	3.0	19.89	Saddle
CTJ159A-1	38	5	2.5	27.3	Crown
CTJ159B-1	38	5	2.5	14.03	Crown
CTJ159B-2	38	5	2.5	13.05	Crown

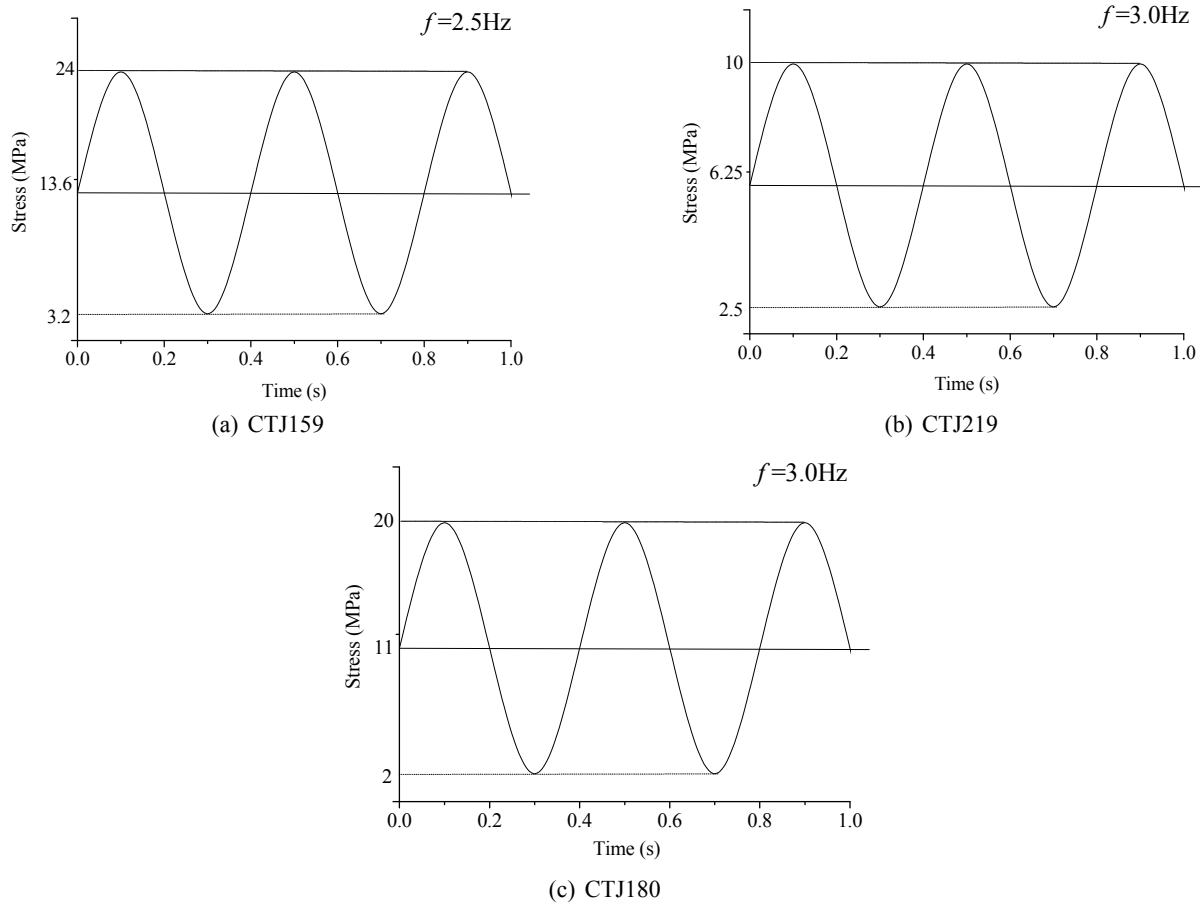


Fig. 7 Schemes of cyclic loading

shown in Figs. 7(a)-(c) for the specimens in the group CTJ159, CTJ219 and CTJ180 respectively. As mentioned previously and illustrated in Fig. 3, each specimen during the fatigue test is pinned at both ends of the chord. Diameter difference between the pin and the hole in the supports exists for the ease of connection between them, which produces a small clearance between the pin and the hole. Such gap can cause oscillation of the specimen and big noise during the fatigue tests. To avoid such phenomenon, the minimum amplitude of the cyclic loading is set to be a little bigger than zero to ensure that the specimen is always in a tensile state and the pin cannot move apart from the edge of the hole. The maximum amplitude of the cyclic loading is designed to produce hot spot stress at the weld toe which is in linear and elastic stage and close to the yield stress of the steel materials. Such loading design can ensure the fatigue tests to be completed quickly. Finally, the loading frequency is not very low to ensure that the fatigue tests are not conducted in a long time. Meanwhile, the loading frequency is not very high to ensure that the test rig has no strong vibration during the fatigue tests.

The crack development during the fatigue test is monitored by using crack gauge as shown in Fig. 8. The crack gauge measures the depth of the fatigue crack located at the weld toe based on alternate current potential drop (ACPD) technique, and such technique was introduced in details by Huang (2002) and Shao and Cao (2005). The accuracy of the crack depth measured by the crack gauge is



Fig. 8 Crack gauge for measuring crack depth and length

in a range of ± 0.1 mm. The loading cycles and the position of the fatigue crack for each specimen in the fatigue test are summarized in Table 4. The location of the fatigue crack, the crack depth a and the crack length $2c$ of all specimens are illustrated in Figs. 9(a)-(h). It is noted here that the crack depth of specimen CTJ219A-2 is very minor (only 0.9 mm) although this specimen also experiences a large number of loading cycles. The possible reason for no crack propagation in specimen CTJ219A-2 may be due to the initiation of another small fatigue crack at the other crown position during the fatigue test. However, the development of the second crack is not monitored during the fatigue test because it is not expected to initiate at this position. The initiation of the second crack may prevent the development of the crack.

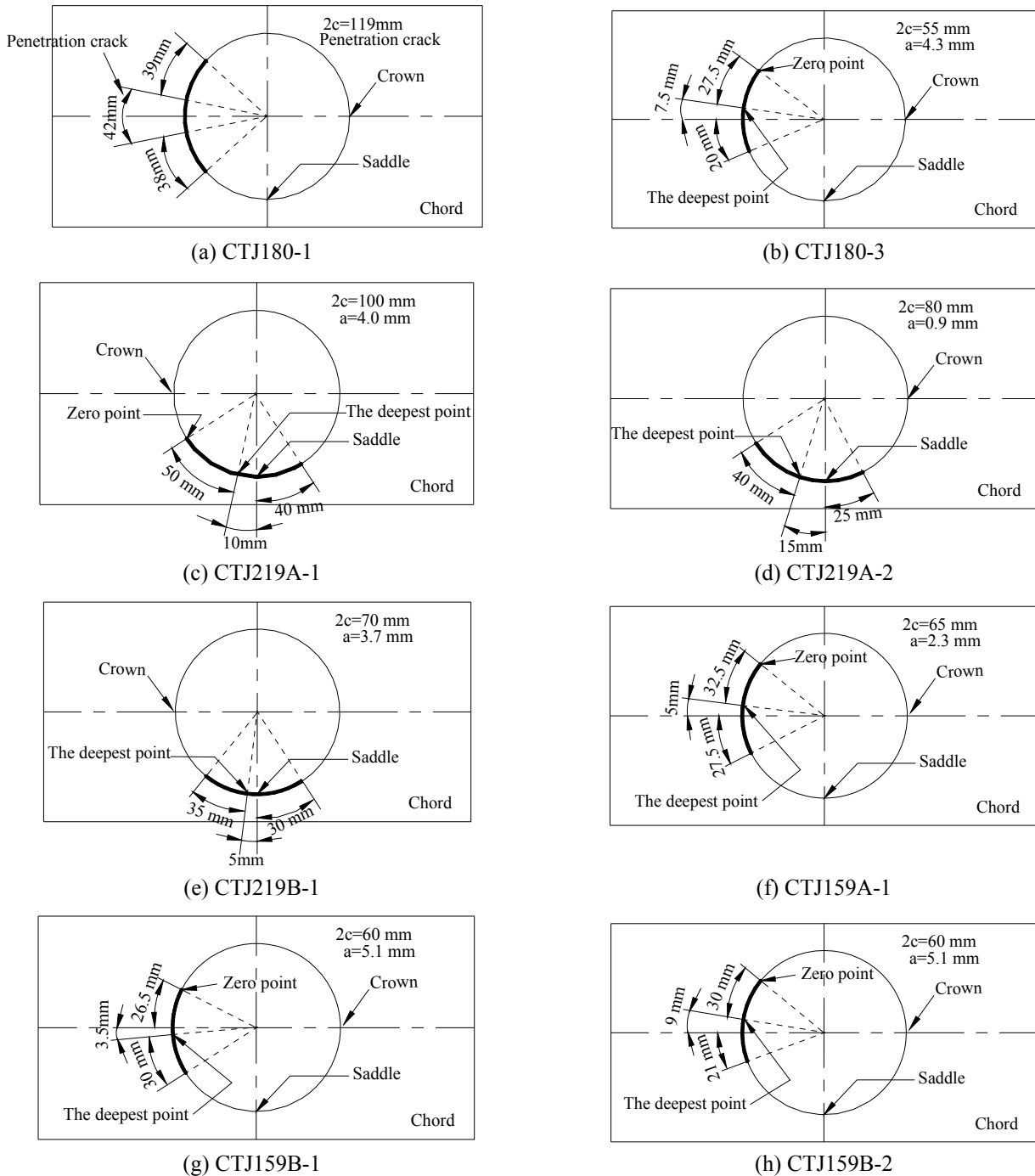


Fig. 9 Details of fatigue crack

From Table 4 and Figs. 9(a)-(h), it is found that the previous prediction on the crack locations for all the specimens is coincident with the experimental observations. Specimen CTJ180-1, which has a lower number of loading cycles at failure, is designed to be subjected to a larger loading amplitude range. The numbers of loading cycles after fatigue tests are found to be much similar for the specimens subjected to same loading cycles in each group. In addition, the fatigue crack in specimen CTJ180-1 already penetrates the chord wall. For other specimens, all the cracks do not penetrate the chord wall after the fatigue tests, i.e., all of them are surface cracks.

4. Static test and results

4.1 Loading process and measurement

The static tests are also carried out in the test rig as shown in Fig. 3. For the specimens with and without fatigue crack, they are subjected to tensile load at the brace end till failure. During the test, an LVDT is placed at the bottom of the mid-span for the chord to measure the displacement as shown in Fig. 10. The displacement at the brace end is recorded automatically during the test by data acquisition system. The difference between the above two displacements



Fig. 10 LVDT at the bottom of the chord

ments is defined as the deformation of the chord, and it also refers to the joint’s ovalisation. Such definition is acceptable because the tension of the brace is much smaller compared to the radial deformation of the chord since the axial stiffness of the brace is generally much bigger than the radial stiffness of the chord.

For the specimens with fatigue crack, the crack development during the static test is also recorded by using the crack gauge. The crack gauge can measure the crack depth along the weld toe to monitor the development of the crack shape. The opening displacement of the crack mouth (CMOD) is observed and measured by using an electron magnifier with a measuring accuracy of 0.1 mm.

In the elastic stage, the load is applied to the specimen in a loading increment of 5 kN/min. After plastic deformation initiates, which can be observed from the load-displacement curve, the load is applied in a displacement increment of 2 mm/min till failure.

4.2 Charpy test

As fatigue crack is located at the weld toe in some specimens, it is necessary to evaluate if the fracture toughness of the steel materials is satisfied with the corresponding specifications (National Standard of the People’s Republic of China 2007). After the static tests, a tube segment cut from the chord in each specimen is used

to fabricate the coupon for Charpy test. The size of the coupon is 10 mm × 5 mm × 55 mm (width × height × length) for the specimens in the group of CTJ219 and 10 mm × 7.5 mm × 55 mm for the specimens in the groups of CTJ159 and CTJ180, as shown in Fig. 11(a). The fractured section of the specimens after impacting tests is shown in Fig. 11(b), and it is found that the fractured section of the specimens in the group of CTJ180 is smooth and bright with very little residual deformation. For the specimens in the groups of CTJ219 and CTJ159, the fractured section is relatively dark and coarse, which indicates that plastic deformation occurs during the impacting tests.

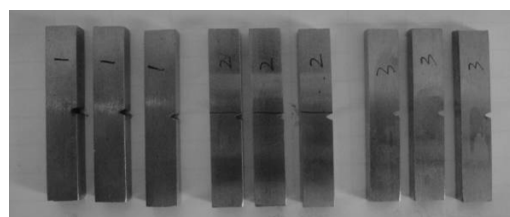
The impact energy of the specimens is listed in Table 5. It is clear that the impact energy for the specimens in the group of CTJ180 is lower than 34 J (the specified minimum value in the corresponding design code (National Standard of the People’s Republic of China 2007)). For the specimens in the groups of CTJ219 and CTJ159, the impact energy is satisfied with the specified value.

4.3 Inclination angle of surface crack

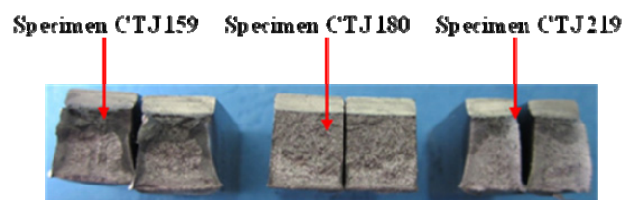
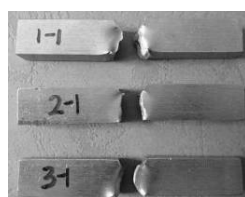
After the static tests, the crack surface is opened, and the crack propagating angle φ , also called the inclination angle of the crack surface as shown in Fig. 12, is also measured.

Table 5 Results from Charpy test

Specimen	Test temperature (°C)	Impact energy (J)
CTJ159-1	20	78
CTJ159-2		68
CTJ159-3		82
CTJ180-1	20	10
CTJ180-2		32
CTJ180-3		10
CTJ219-1	20	50
CTJ219-2		50
CTJ219-3		50



(a) Before test



(b) After test

Fig. 11 Specimens in Charpy test

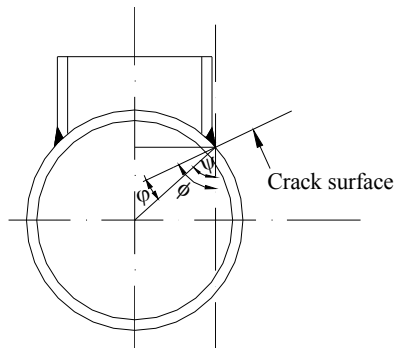


Fig. 12 Inclination angle of a crack in a tubular joint

Table 6 Measured inclination angles of crack surface

Group	Specimen	ϕ (°)	Averaged ϕ (°)	Position	φ (°)
CTJ180	CTJ180-1	5.0	5.75	Crown	5.75
	CTJ180-2	*			
	CTJ180-3	6.5			
CTJ219	CTJ219A-1	38.0	37.75	Saddle	8.2
	CTJ219A-2	*			
	CTJ219B-1	37.5			
CTJ159	CTJ159A-1	13.5	14.5	Crown	14.5
	CTJ159B-1	14.0			
	CTJ159B-2	16.0			

Note: *inclination angle is not measured

In Fig. 12, ψ is the angle between the vertical direction and the direction of the line passing through the weld toe and the centroid of the chord's cross section. ϕ is the angle between the vertical direction and the direction of the line passing through the weld toe and the actual crack surface. The inclination angle of the fatigue crack φ is then calculated from the following equation

$$\varphi = \phi - \psi \quad (1)$$

The measured results of the inclination angle of the crack surface for all the cracked specimens are summarized in Table 6. It can be seen from the measured results that the inclination angle of the crack surface is influenced by the brace-to-chord diameter ratio β . For a tubular T-joint with a bigger value of β , the inclination angle is smaller.

The inclination angles for the cracked specimens indicate that previous modelling technique for the surface crack in tubular joints by some researchers (Borges

et al. 2012, Lee *et al.* 2005) is not absolutely accurate since it is assumed $\varphi = 0^\circ$ in their studies. However, the maximum value of φ for all the specimens is about 15° . In previous study (Shao 2005), the effect of the inclination angle on the stress intensity factor was investigated, and it was found that the stress intensity factor of the surface crack with an inclination angle of 15° in a tubular joint has a difference of less than 10% compared to the result of the surface crack perpendicular to the chord surface. Hence, such effect is minor when the inclination angle is less than 15° .

4.4 Failure mode

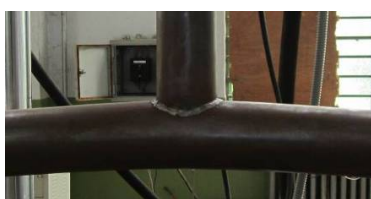
4.4.1 Uncracked specimens

The failure modes of the specimens without fatigue crack (CTJ159B-3, CTJ180-4, CTJ219-B2) are shown in Figs. 13(a)-(c) respectively. For the three uncracked specimens, the final failure modes are all plastic yielding around the weld toe. However, the failure mechanism is not absolutely same for each specimen. Specimen CTJ180-4, which has a big value of β (0.739), has a clear residual flexural deformation of the chord after the static test as shown in Fig. 13(a), which implies that this specimen behaves much like a bending beam for the chord. When the value of β is smaller, such as the specimens CTJ159B-3 ($\beta = 0.28$) and CTJ219B-2 ($\beta = 0.493$), local plastic failure around the weld toe on the chord surface is the dominant failure mode as shown in Figs. 13(b) and (c). In this case, the flexural deformation of the chord is relatively smaller, and the ovalization of the chord in the brace/chord connection region is much clear.

In overall, for the tubular T-joints without fatigue crack, no fracture failure occurs when they are subjected to axial tensile load at the brace end, and plastic failure becomes the main failure mechanism although such plasticity may appear in different forms when the geometry of the joints is different.

4.4.2 Specimens with fatigue crack in group of CTJ180

For the specimen CTJ180-1, the maximum stress at the weld toe in the cyclic loading exceeds the yield strength of the steel material, and hence the fatigue crack propagates very fast. After the fatigue test, it is found that the crack already penetrates the chord wall. In the static test, the specimen is suddenly fractured in the chord and the crack propagates very fast along its two ends when the load exceeds a critical value. The final failure mode is shown in Fig. 14(a). For the other two specimens CTJ180-2 and



(a) CTJ180-4



(b) CTJ159B-3



(c) CTJ219B-2

Fig. 13 Failure mode of uncracked specimens

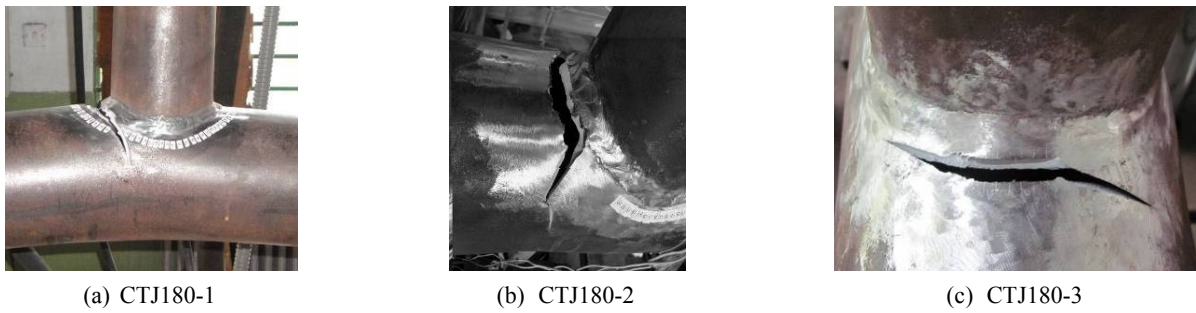


Fig. 14 Failure mode of cracked specimens in group CTJ180

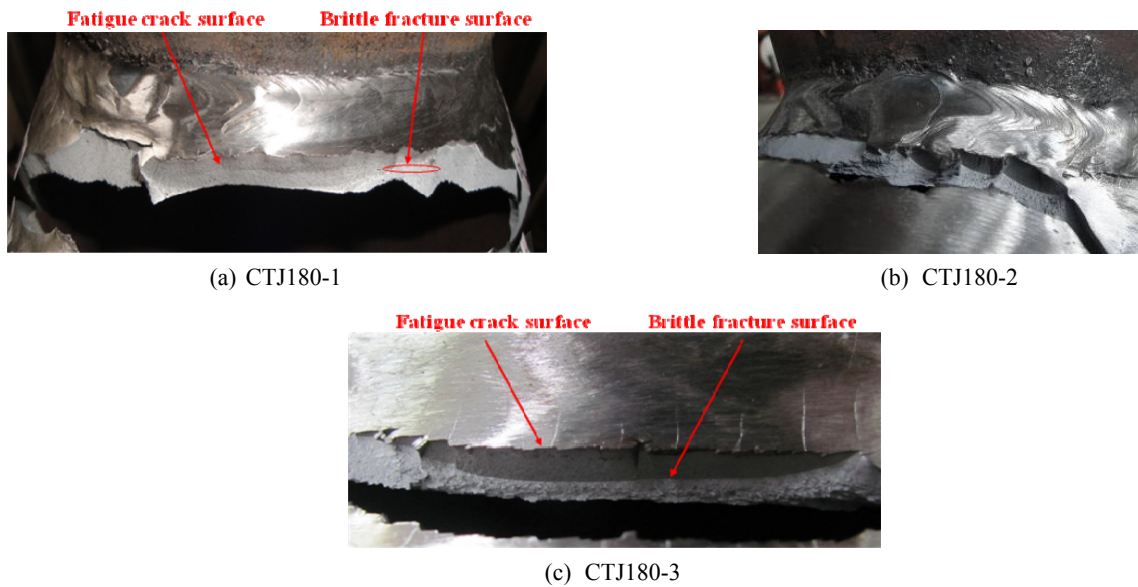


Fig. 15 Crack surfaces of the specimens in group CTJ180

CTJ180-3, the cracks are not penetrating through the entire chord wall after the fatigue tests. In the static tests, the two specimens are also suddenly fractured at critical loads, and the final failure modes of the two specimens are shown in Figs. 14(b) and (c).

From Figs. 15(a)-(c), it can be found that the crack surfaces of the specimens CTJ180-1 and CTJ180-3 can be divided into two types: a dark and smooth surface produced from the fatigue test, and a bright and rough surface caused by brittle fracture. No clear ductile shear crack surface is found from the observations. For specimen CTJ180-2, the crack surface is not observed because the crack surface is very rough.

However, it should be noted that all of the specimens in the group of CTJ180 experience large plastic deformation in the chord before final fracture because large residual deformation of the chord is observed after the static test, which implies that the cracked specimens in the group of CTJ180 still have a large capacity of plastic deformation in the chord before final fracture.

4.4.3 Specimens with fatigue crack in group of CTJ219

In the three specimens of the group of CTJ219, specimen CTJ219A-2 has a very small crack depth compared to the other two specimens, and the crack depth



Fig. 16 Failure modes of the specimens in group CTJ219

of specimen CTJ219B-1 is smaller than that of specimen CTJ219A-1. During the static test, it is found that specimen CTJ219A-2 experiences a very large plastic deformation in the chord while no clear crack propagation is observed, as shown in Fig. 16(b). For specimen CTJ219A-1, the crack is propagating continuously during the loading process till it penetrates the chord wall as shown in Fig. 16(a). It is also observed from Fig. 16(a) that the chord ovalisation of the specimen is already very clear when the crack penetrates the chord wall. The failure mode of specimen CTJ219B-1 is observed from Fig. 16(c), in which it is clear that both the chord ovalisation and the chord's bending deformation are very big after the static test. However, it is measured from the crack gauge that the crack does not penetrate the chord wall although it propagates to a large depth.

After the static tests, specimens CTJ219A-1 and CTJ219B-1 are splitted into two parts along the crack surface at the weld toe to observe the crack propagating process. The crack development in the two specimens can be seen in Figs. 17(a) and (c). Because only a small crack with much minor depth is located in specimen CTJ219A-2 and no crack propagation is monitored during the static test, specimen CTJ219A-2 cannot be splitted just from tensile loading at the brace end. However, it can be found from Fig. 17(b) that only a slight opening of the crack mouth is observed after the static test.

It is clear that the crack propagation of the specimens in the group of CTJ219 (except CTJ219A-2) is much different with the crack development of the specimens in the group of CTJ180. As seen from Fig. 17(a), the crack surface of specimen CTJ219A-1 during the static test includes three different sections: fatigue crack surface, ductile crack surface and brittle crack surface. The fatigue crack surface is dark and smooth, and it is produced during fatigue test before the static test. The ductile crack surface, which is also relatively smooth and bright, is produced during the static test before final sudden fracture failure. The brittle crack surface is produced suddenly after the load is increased to a critical value. The sudden fracture causes the

brittle crack surface to be rough and bright. In specimen CTJ219B-1, the fatigue crack also propagates in the thickness direction of the chord wall during the static test. However, no brittle failure occurs in this specimen before the test is finished, which may be due to the smaller crack depth compared to specimen CTJ219A-1. After the static test, the specimen is loaded till the fatigue crack is splitted into two separate surfaces suddenly as shown in Fig. 17(c). The final crack in Fig. 17(c) is clearly consisted of three surfaces: fatigue crack surface, ductile crack surface and brittle crack surface. Similarly, the fatigue crack surface and the ductile crack are produced in the fatigue test and in the static test respectively. The brittle crack surface, not produced in the static test, is generated artificially after the static test.

Based on the above analyses, it is found that good plasticity is assured for the specimens in the group of CTJ219 during the static test. Ductile crack development exists in both specimens of CTJ219A-1 and CT219-B1.

4.4.4 Specimens with fatigue crack in group of CTJ159

The final failure modes of the specimens in the group of CTJ159 are illustrated in Figs. 18(a)-(c). For specimen CTJ159A-1, both local ovalisation and bending deformation of the chord are quite big as shown in Fig. 18(a). When the load is increased to a critical value, a brittle fracture occurs suddenly. Similar failure process occurs for the other two specimens as shown in Fig. 18(b) and (c).

From the careful observation for the crack surfaces of the three specimens, as shown in Figs. 19(a)-(c), the crack surface includes two clear parts: fatigue crack surface and brittle crack surface. Although the toughness of the steel materials is satisfied with the specification in Chinese code (National Standard of the People's Republic of China 2007), these specimens also show a final brittle fracture failure, which is different with the observations for the specimens in the group of CTJ219. This may be caused by the geometry of the specimens. The brace-to-chord diameter

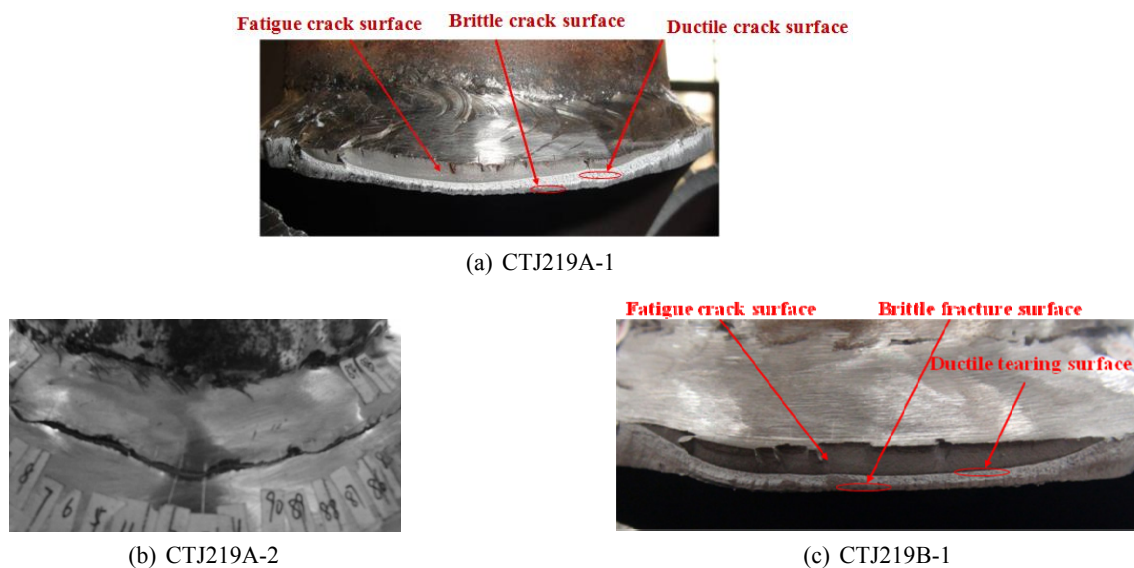


Fig. 17 Crack surfaces of the specimens in group CTJ219

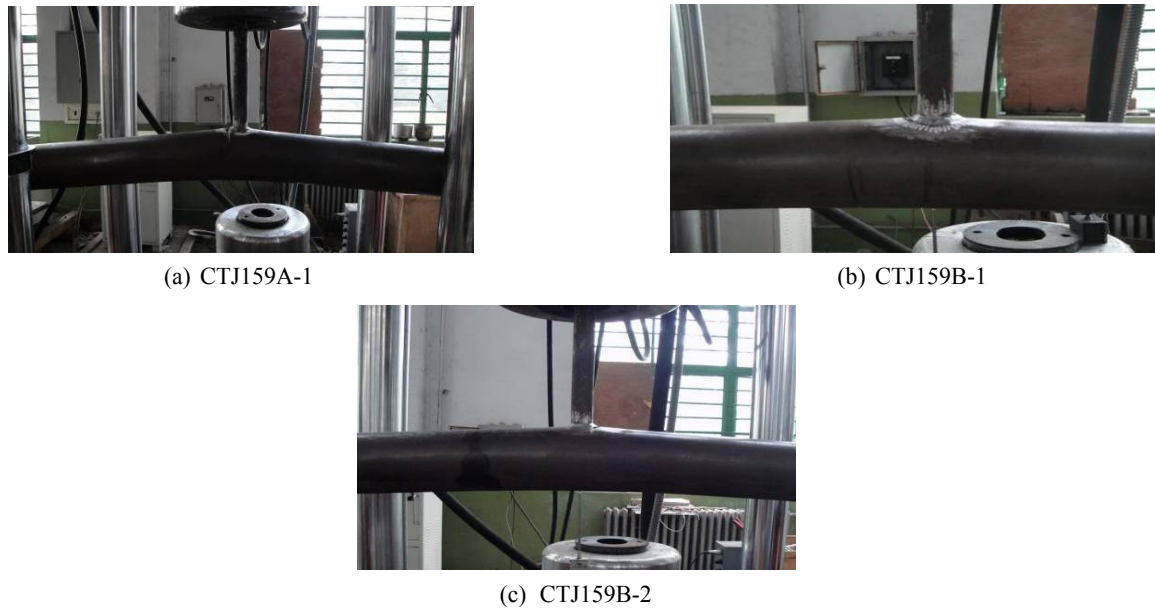


Fig. 18 Failure modes of the specimens in group CTJ159

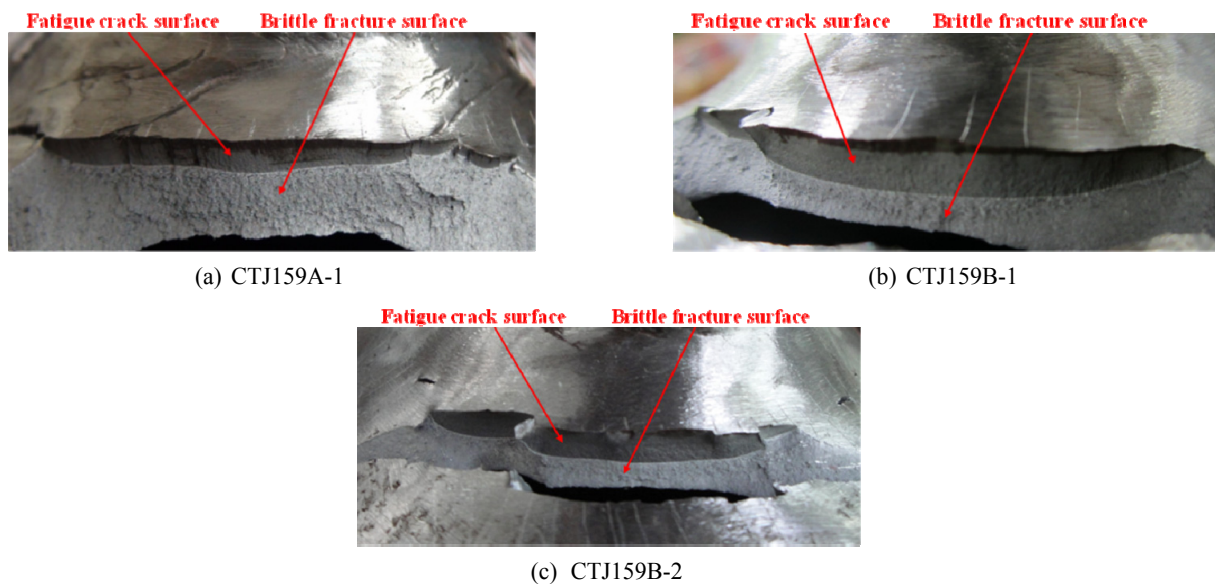


Fig. 19 Crack surfaces of the specimens in group CTJ159

ratio β is the only different geometrical parameter in the specimens between the groups of CTJ219 and CTJ159. A smaller value of β definitely causes more severe stress concentration at the weld toe in a tubular T-joint. As tri-axial stress state exists easily in a region with high stress gradient caused by severe stress concentration, such stress state causes the material to become much more brittle, and thus it is more sensitive for the T-joint to lose its loading carrying capacity in fracture failure.

4.5 Crack development

The crack development is monitored by using crack gauge in the static test. For the specimens in the group of CTJ180, the measured crack developments for specimens CTJ180-1 and CTJ180-3 are shown in Figs. 20(a) and (b)

respectively. For specimen CTJ180-2, the measured data is lost and the crack development is hence not provided here. As the fatigue crack in specimen CTJ180-1 already penetrates the chord wall, the crack's propagation is mainly towards its two tips as shown in Fig. 20(a). It is different from previous reported studies (Talei-Faz *et al.* 2004, Zerbst *et al.* 2002) because the cracks in the specimens were all surface cracks. In the thickness direction of the chord wall, the crack seems to propagate slowly. As mentioned previously, the measurement of the crack depth is based on an ACPD (alternate current potential drop) technique. When the crack penetrates the chord wall, the measured crack depth is not accurate, and thus the crack propagation in Fig. 20(a) cannot be used reliably in evaluating the crack development in the thickness direction of the chord wall. However, the crack propagation at the two tips can be

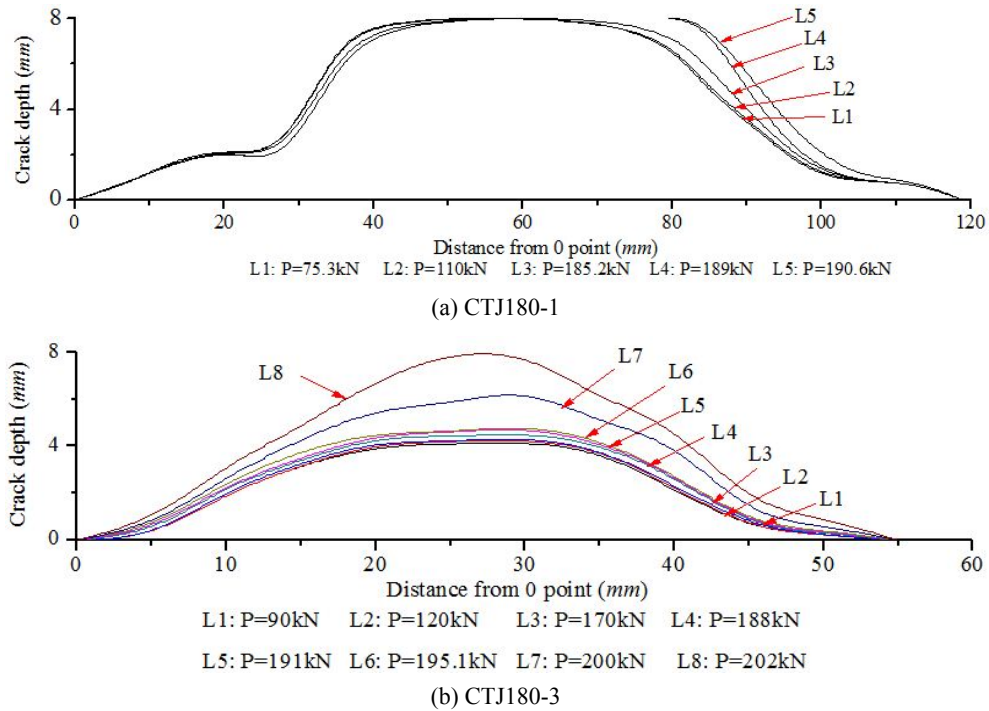


Fig. 21 Crack development for specimens in group CTJ219

captured relatively accurately. For specimen CTJ180-3, the crack development is much different. The crack seems to propagate very slowly before curve L6 although the load is increased continuously. However, the crack propagates suddenly with a large increasing magnitude in the thickness direction of the chord wall from L6 to L7 although the increase of the applied load is minor, which indicates that a brittle rather than ductile fracture occurs.

For the specimens in the group of CTJ219, the crack developments are illustrated in Figs. 21(a)-(c). Such crack

developments are much different because all the cracks in the three specimens propagate steadily with a small increment of the crack depth during the static test. For specimen CTJ219A-2, the crack propagation in the depth is very slight due to the effect of the other shallow crack located in the opposite crown position. For the other two specimens, no brittle fracture failure occurs during the whole static tests since no sharp increase of the crack depth is observed in the crack development, which is coincident with the observations as shown in Figs. 17(a) and (c).

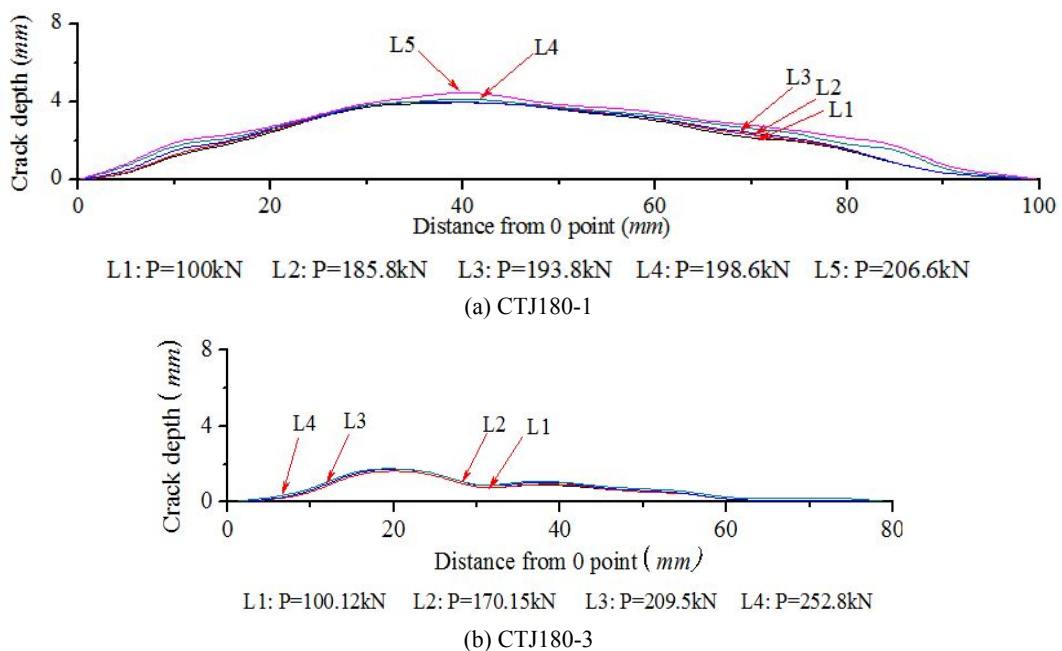
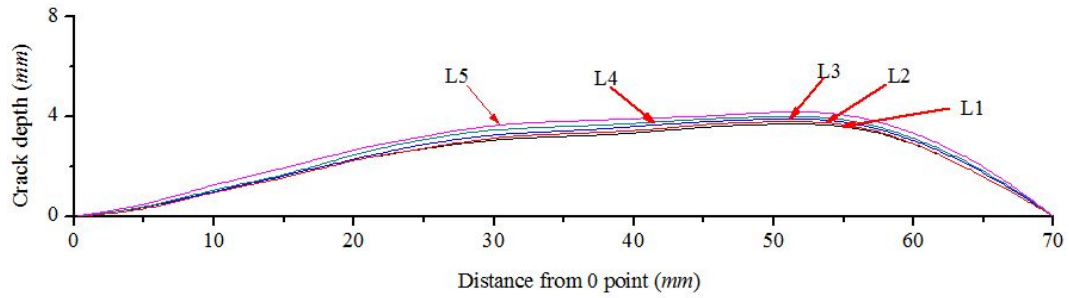


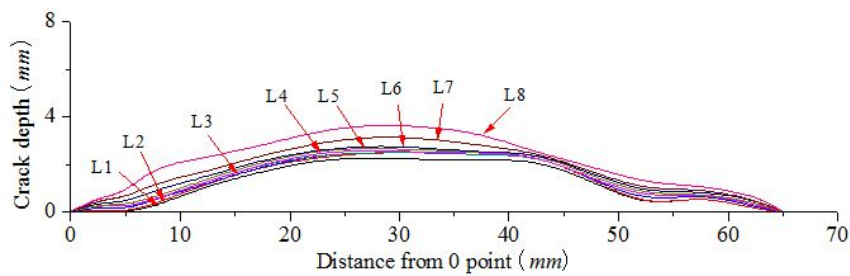
Fig. 21 Crack development for specimens in group CTJ219



L1: P=30kN L2: P=90.22kN L3: P=120kN L4: P=140kN L5: P=165kN

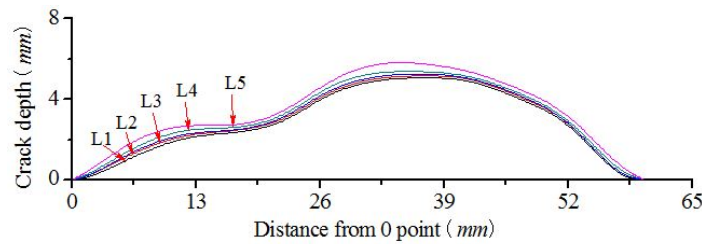
(c) CTJ219B-1

Fig. 21 Continued



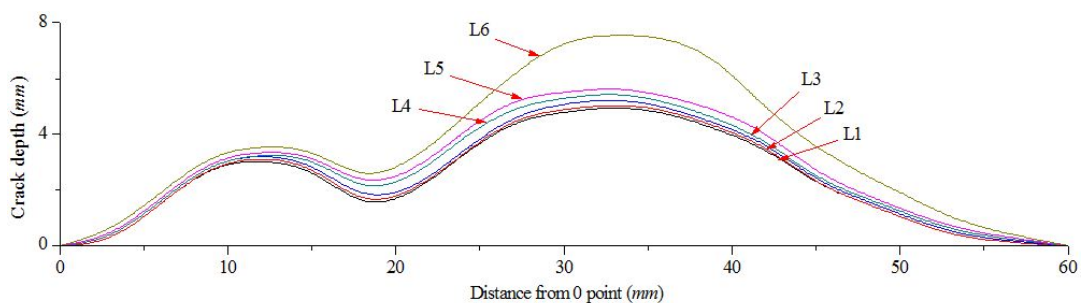
L1: P=80kN L2: P=100.05kN L3: P=121.5kN L4: P=133kN L5: P=138.6kN
L6: P=142kN L7: P=145kN L8: P=148kN

(a) CTJ159A-1



L1: P=60kN L2: P=100kN L3: P=110kN L4: P=124kN L5: P=125kN

(b) CTJ159B-1



L1: P=30kN L2: P=90.15kN L3: P=114.7kN L4: P=121kN L5: P=126kN L6: P=124.6kN

(c) CTJ159B-2

Fig. 22 Crack development for specimens in group CTJ159

Generally, the crack developments of the three specimens in the group of CTJ159 are similar to those of the specimens in the group of CTJ180, as shown in Figs. 22(a)-(c). There is a gradually propagating process before final fracture failure in the static tests. When the crack depth exceeds to a certain value, a fast crack propagation occurs with a minor increase of the load to show that a

brittle fracture failure occurs along the crack tip (from L6 to L7 for specimen CTJ159A-1, from L5 to L6 for specimen CTJ159B-2, and from L4 to L5 for specimen CTJ159B-1).

4.6 Opening displacement of crack mouth (CMOD)

The crack development can be also evaluated from the

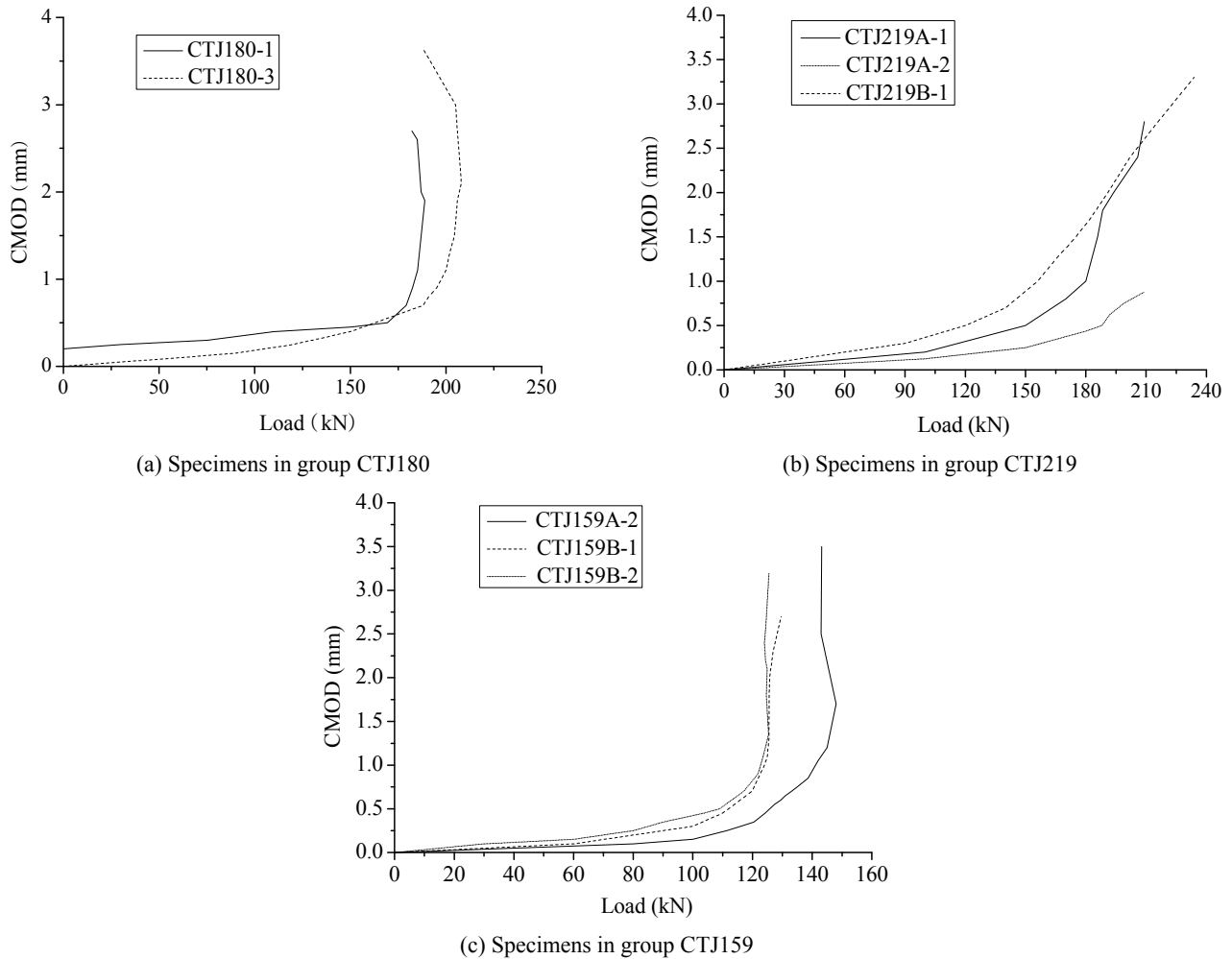


Fig. 23 Opening displacement of crack mouth development

CMOD-load curve for each specimen. For all the specimens in the static tests, the CMOD-load curves are plotted in Figs. 23(a)-(c). It should be noted here that CMOD in Figs. 23(a)-(c) is the maximum value along the crack length. Generally, the CMOD-load curves can be classified into two principal stages: approximately linear stage and clearly nonlinear stage. In the approximately linear stage, the CMOD is increasing with the increase of the applied axial load, and the relationship between them is close to be linear. In this stage, the fatigue crack opens in a linear and elastic state, and hence the CMOD is proportional to the applied load. Plastic deformation only exists in a small region around the crack tip. With the increase of the applied load, the plastic region around the crack tip becomes larger, and the crack becomes blunted. In this case, the value of the CMOD increases quickly with relatively minor loading increment, and this stage is defined as the nonlinear stage. A blunted crack is much more feasible to propagate in a ductile form, and it occurs more easily when the toughness of the steel material is high and stress concentration is not much severe at the crack tip.

According to the observations for the crack surfaces in the specimens as shown in Figs. 15, 17 and 19, ductile crack surface only exists in the specimens in the group of CTJ219 while there is almost no evidence for a ductile crack surface

in the specimens in the groups of CTJ180 and CTJ159. Such observations also support the CMOD-load curves of these specimens. In Figs. 23(a) and (c), it is clear that the CMOD almost increases in an upward direction in the nonlinear stage for the specimens in the groups of CTJ180 and CTJ159, and a load drop can be found after the COMD is beyond a critical value. The above phenomenon implies that the CMOD increases sharply with almost no increase of the load. This situation occurs due to the brittle fracture failure because the specimens cannot sustain an increasing load at such state. However, the CMOD increases gradually with the increase of the load for the specimens in the group of CTJ219 as shown in Fig. 23(b), and there is no sharp increase of the CMOD within a slight loading increase. This phenomenon is caused by a ductile crack propagation rather than a brittle fracture failure process. The development of CMOD of specimens in group CTJ180 and CTJ159 in the second stage is much different with previous studies (Talei-Faz *et al.* 2004, Zerbst *et al.* 2002) in which ductile tearing process of the surface cracks in the specimens were observed and measured.

4.7 Load carrying capacity

The load carrying capacity of a circular tubular joint,

also called the static strength, can be determined from different methods. One method is based on the load-displacement curve and the other method is on basis of the load-ovalisation curve. The determination on the load carrying capacity of a tubular joint from the load-displacement curve is referred to a twice elastic compliance criterion as shown in Fig. 24. A straight line passing through a point at the load-displacement curve has an angle

to the vertical axis (load) of ω_1 and the tangential line in the linear stage of the curve has an angle to the vertical axis of ω_2 . If the two angles satisfy the following relationship

$$\tan \omega_1 = 2 \tan \omega_2 \quad (2)$$

Then the load carrying capacity of the tubular joint is determined from the corresponding load at the point on the load-displacement curve as shown in Fig. 24.

For another definition from the load-ovalization curve, Lu's limit (Lu *et al.* 1994) is used to determine the load carrying capacity of a tubular joint from an ovalisation of 3% of the chord diameter. As the chord ovalization for some specimens in the static test is not very big, this definition is not selected in this study. Therefore, the twice elastic compliance criterion is used for determining the load carrying capacity of the tubular T-joints.

The experimental results of the load-displacement curves for all the specimens are plotted in Figs. 25(a)-(c). For the specimens in the group of CTJ180 as shown in Fig. 25(a), the load-displacement curves of the cracked specimens all have a peak point, and the load reduces due to brittle fracture after that point. For the uncracked specimen, there is no peak point on the load-displacement curve although a knee point exists to indicate the nonlinear stage.

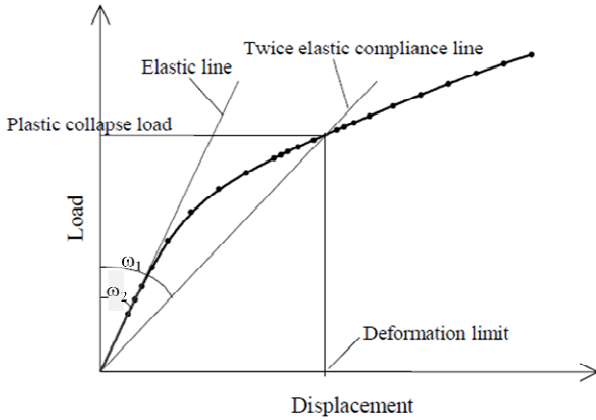
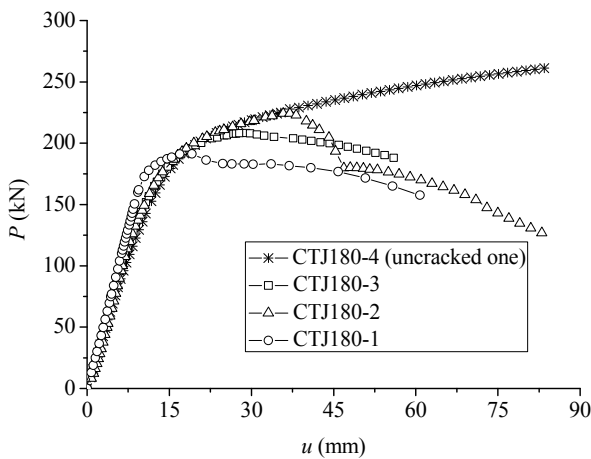
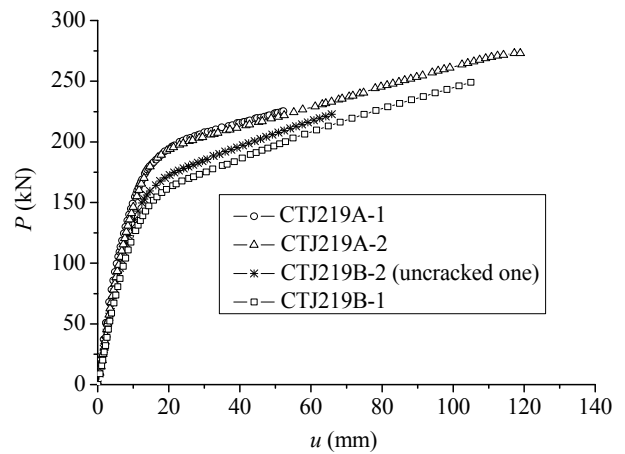


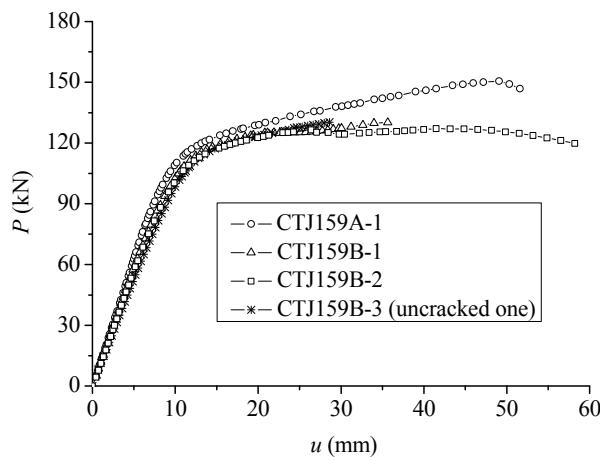
Fig. 24 Twice elastic compliance criterion



(a) Specimens in group CTJ180



(b) Specimens in group CTJ219



(c) Specimens in group CTJ159

Fig. 25 Load-displacement curves

For the specimens in the group of CTJ219 as shown in Fig. 25(b), the load-displacement curves of both uncracked and cracked specimens have no peak points, and only knee points are found to be located at the curves, which proves that no brittle fracture occurs in the static tests. For the specimens in the group of CTJ159, it is found that there is also a load drop in the load-displacement curve for the cracked specimens. However, such load drop is relatively much minor and it occurs at a very large displacement.

The loading drop after the peak value for the specimens in group CTJ180 as shown in Fig. 25(a) indicates that the through crack has effect on both failure load and failure mechanism, which is different from the reported conclusions of previous studies (Talei-Faz *et al.* 2004, Zerbst *et al.* 2002) that surface crack has very minor effect on the static strength and the failure of the specimens containing crack is ductile.

According to the definition of the twice elastic compliance criterion on the load carrying capacity of a tubular joint, the load carrying capacities of all the specimens are generalized in Table 7. P_u and P_c in table represent the load carrying capacities of the specimens without and with fatigue crack respectively. For the specimens in the group of CTJ180, the load carrying capacities of all the cracked specimens decrease. However, the decreasing magnitude for specimen CTJ180-1 is much bigger because the fatigue crack already penetrates the chord wall. For the other two specimens, the decrease of the load carrying capacity is much slight, which implies that the surface crack has a minor influence on the static strength.

For the specimens in the group of CTJ219, it is found that the decrease of the load carrying capacity for the cracked specimen CTJ219B-1 is also slight because such decrease is only 3.4%. For the cracked specimens, CTJ219A-1 and CTJ219A-2, the load carrying capacity has an increase rather than a decrease although there is a fatigue crack located at the weld toe. This abnormal phenomenon is produced due to the different material properties (mainly the yield strength) as listed in Table 2. The yield strength of the steel materials for specimens CTJ219A-1 and CTJ219A-2 is 322 MPa while such value for specimen CTJ219B-2 is 290.2 MPa. According to the presented equations in some design guidelines (IIW 1999, Wardenier *et al.* 2008), the static strength of tubular T-joints under axial loading is proportional to the yield strength of the steel materials. Based on this conclusion, the load carrying capacities of the specimens CTJ219A-1 and CTJ219A-2 are 178.0 kN and 179.2 kN respectively if the yield strength of the two specimens are also 290.2 MPa. In this case, the static strengths of the two cracked specimens are almost same as that of the uncracked specimen CTJ219B-2 although such values are still slightly bigger. The slight difference may be caused by other fabrication difference such as the weld size. In overall, it seems that the cracked specimens have very slight decrease in the load carrying capacity. Similarly, it is also found that the load carrying capacities of the cracked specimens CTJ159B-1 and CTJ159B-2 also have a slight decrease compared to the static strength of the uncracked specimen CTJ159B-3. A slightly bigger value of the load carrying capacity for

Table 7 Results of static test

Specimen	Crack type	Crack position	Load carrying capacity (kN)		$(P_u - P_c) / P_u$
			P_u	P_c	
CTJ180-1	Through crack	crown	—	186.0	14.1%
CTJ180-2	Surface crack	crown	—	215.4	0.5%
CTJ180-3	Surface crack	crown	—	207.2	4.3%
CTJ180-4	—	—	216.5	—	—
CTJ219A-1	Surface	saddle	—	197.4	-13.3%
CTJ219A-2	Surface	saddle	—	198.8	-13.9%
CTJ219B-1	Surface	saddle	—	168.3	3.4%
CTJ219B-2	—	—	174.2	—	—
CTJ159A-1	Surface	crown	—	130.1	-3.2%
CTJ159B-1	Surface	crown	—	124.2	1.5%
CTJ159B-2	Surface	crown	—	124.9	0.9%
CTJ159B-3	—	—	126.1	—	—

Table 8 Load carrying capacities from tested and predicted results

Specimen	$P_{uncrack}$ (kN)	F_{AR}	P_{crack}^{AR} (kN)	P_{crack}^{Test} (kN)	$(P_{crack}^{Test} - P_{crack}^{AR}) / P_{crack}^{Test} \times 100\%$
CTJ180-1	216.5	0.832	180.1	186.02	3.18%
CTJ180-3	216.5	0.920	199.025	207.24	3.96%
CTJ219B-1	174.2	0.935	162.83	174.22	6.54%
CTJ159B-1	126.1	0.897	113.05	124.16	11.11%
CTJ159B-2	126.1	0.915	115.31	124.91	7.69%

cracked specimen CTJ159A-1 compared to the uncracked specimen CTJ159B-3 is also caused by the different material properties of the steels. By using the same equivalent method after reducing the yield strength of the steel material, the static strength of the cracked specimen CTJ159A-1 is 119.7 kN. In this case, the load carrying capacity of cracked specimen CTJ159A-1 is decreased by 5.1% compared to the corresponding value of the uncracked specimen CTJ159B-3.

Based on the above analyses, it is found that a surface crack in a tubular T-joint seems to have a slight influence on the load carrying capacity. However, the effect of a penetration crack on the load carrying capacity of a tubular T-joint is remarkable and it cannot be neglected.

In theory, the residual strength of a cracked tubular joint was reported to be estimated from an area reduction factor F_{AR} in the literature (HSE 2002, BS7910 2013). In this method, the load carrying capacity of a cracked tubular joint, P_{crack} , is calculated from the following equation

$$P_{crack} = F_{AR} \cdot P_{uncrack} \quad (3)$$

where $P_{uncrack}$ is the load carrying capacity of the corresponding uncracked tubular joint.

F_{AR} , as reported in HSE (2002) and BS7910 (2013), is expressed as follow

$$F_{AR} = \left(1 - \frac{A_{crack}}{T \times \text{weld length}} \right) \frac{1}{Q_{\beta}} \quad (4)$$

Where A_{crack} is the area of the fatigue crack.

Q_{β} in Eq. (4) is calculated from the following equation

$$Q_{\beta} = \begin{cases} 1.0 & (\beta \leq 0.6) \\ \frac{0.3}{\beta(1-0.833\beta)} & (\beta > 0.6) \end{cases} \quad (5)$$

The tested static strengths of the specimens in the groups of CTJ180, CTJB219 and CTJ159B are used to evaluate the reliability of the above theory, and the tested results together with the predicted results from the above equations are listed in Table 8.

It is found from Table 8 that Eqs. (3)-(5) generally provides conservative estimation for the load carrying capacity of the cracked specimens because the predicted results are lower than the tested results. The relative error between the predicted and the tested results is less than 10% for most cracked specimens except specimen CTJ159B-1. It seems that the accuracy of Eqs. (3)-(5) is higher when parameter β has a bigger value. With the decrease of β , the predicted result becomes more conservative.

4.8 Discussion on influence of fatigue crack on integrity of cracked tubular joints

Although the influence of the surface crack on the load carry capacity is minor for the specimens in the static tests, cautions are still necessary to be taken when the safety evaluation for cracked tubular T-joints is carried out due to the following several reasons: (1) The load carrying capacities of the cracked specimens are determined from the

load-displacement curve based on the twice elastic compliance criterion. It is found that the points corresponding to the load carrying capacity in the load-displacement curves for the specimens in the group of CTJ180 are located at a position before the load decreasing stage, which implies that the specimens may fail suddenly after the static strength. The determined load carrying capacity cannot be used to predict the final failure mode of these specimens. Once these specimens are suffered from a surcharge loading, there is no potential strength for the joint to sustain such surcharge load. (2) The materials of the specimens in the group of CTJ180 have lower toughness, and it seems that such low toughness causes brittle fracture failure of the cracked specimens. Therefore, the toughness of the steel material is also an important factor necessary to be considered. As the materials of the specimens are all carbon steel with a relatively good toughness, the failure process of tubular T-joints made of high strength steels is important to be investigated because high strength steels generally have lower toughness. (3) It seems that the joint's geometry also has an influence on the final failure mode based on the observations of the different crack surfaces for the specimens in the groups of CTJ219 and CTJ159 even all of these specimens have satisfied toughness. (4) Although the surface crack seems to have slight effect on the static strength of tubular T-joints, it has really remarkable effect on the fatigue life. Once a fatigue crack initiates, the tubular joint may be fail in a short servicing time due to the fast propagation of such fatigue crack.

Another point stated here is the scaling issue of the specimens. Due to the limitation of the test rig, reduced-scale specimens were tested in this study. In the tubular structures used in offshore platform, the thickness of the steel tube is much bigger. The thickness of the steel tube has influence on the failure mechanism of welded tubular joints from the following two aspects: (1) The fracture toughness of the steel material is related to the thickness of the tube. The fracture toughness of the steel material is only steady when the wall thickness of the steel tube is bigger than a critical value. However, such critical thickness is dependent on the types of steel materials, and corresponding tests are necessary to determine such value. (2) When the thickness of the steel tube is bigger, residual stress at the weld may become severe. Large residual stress is harmful to the fracture toughness of the steel materials. Due to the above reasons, more tests on full-scale tubular joints are necessary to be carried out in the future to observe if similar results and conclusions are obtained.

5. Conclusions

Based on static tests on circular tubular T-joints with fatigue crack, the following conclusions can be obtained:

- (1) The geometry of a tubular T-joint influences the location of the peak hot spot stress, and thus it influences the location of the fatigue crack initiation. Additionally, the geometry of a tubular T-joint also influences the propagating direction of the crack surface.

- (2) When the fatigue crack does not penetrate the chord wall and the crack depth ratio of a/T is less than 0.67, it has slight effect on the load carrying capacity of a circular tubular T-joint made of carbon steel. However, a through crack has a very remarkable effect.
- (3) The toughness of the steel materials and the brace-to-chord ratio (β) of tubular T-joints have disadvantageous effect on the crack propagation because nearly no ductile crack surface is observed from the final crack surface.
- (4) The specimens tested in this study are reduced-scale ones, and full-scale specimens are recommended to be tested in future research work because the fracture toughness of a welded thick tube wall is different and it may produce influence on the failure mode of cracked tubular T-joints.

References

- Bjork, T., Marquis, G. and Heinila, S. (2008), "Assessment of subzero fracture of welded tubular K-joint", *J. Struct. Eng., ASCE*, **134**(2), 181-188.
- Borges, L., Chiew, S.P., Nussbaumer, A. and Lee, C.K. (2012), "Advanced numerical modelling of cracked tubular K-joints: BEM and FEM comparison", *J. Bridge Eng.*, **17**(3), 432-442.
- BS7910 (2013), Guide to methods for assessing the acceptability of flaws in metallic structures; BSI Standards Publication, UK.
- Chiew, S.P., Lie, S.T., Lee, C.K. and Huang, Z.W. (2004), "Fatigue performance of cracked tubular T-joints under combined loads. I: Experimental", *J. Struct. Eng., ASCE*, **130**(4), 562-571.
- Chiew, S.P., Lee, C.K., Lie, S.T. and Nguyen, T.B.N. (2009), "Fatigue study of partially overlapped CHS K-joints. Part II: experimental study and validation of numerical models", *Eng. Fract. Mech.*, **76**(16), 2408-2428.
- Cui, M.J. and Shao, Y.B. (2015), "Residual static strength of cracked concrete-filled circular steel tubular (CFCST) T-joint", *Steel Compos. Struct., Int. J.*, **18**(4), 1045-1062.
- Fathi, A. and Aghakouchak, A.A. (2007), "Prediction of fatigue crack growth rate in welded tubular joints using neural network", *Int. J. Fatigue*, **29**(2), 261-275.
- Hanji, T., Park, J.E. and Tateishi, K. (2014), "Low cycle fatigue assessment of corner welded joints based on local strain approach", *Int. J. Steel Struct.*, **14**(3), 579-587.
- HSE (2002), The static strength of cracked joints in tubular members; Offshore Technology Report, UK.
- Huang, Z.W. (2002), "Stress intensity factor of cracked steel tubular T and Y-joints under complex loads", Ph.D. Thesis; Nanyang Technological University, Singapore.
- International Institute of Welding (IIW) (1999), Recommended Fatigue Design Procedure for Hollow Section Joints: Part 1-Hot Spot Stress Method for Nodal Joints, IIW Doc. XV-1035-99, XV-E-99-251, XIII-1804-99, Lisbon, Portugal, July.
- Jia, L.J. (2014), "Effect of post weld treatment on cracking behaviors of beam-column connections in steel bridge piers", *Steel Compos. Struct., Int. J.*, **17**(5), 685-702.
- Jia, L.J., Ikai, T., Kang, L. and Kato, T. (2016), "Ductile cracking simulation procedure for welded joints under monotonic tension", *Struct. Eng. Mech., Int. J.*, **60**(1), 51-69.
- Jiki, P.N. and Agber, J.U. (2014), "Damage evaluation in gap tubular truss 'K' bridge joints using SFEM", *J. Constr. Steel Res.*, **93**, 135-142.
- Lee, C.K., Lie, S.T., Chiew, S.P. and Shao, Y.B. (2005), "Numerical models verification of cracked tubular T, Y and K-joints under combined loads", *Eng. Fract. Mech.*, **72**(7), 983-1009.
- Lie, S.T. and Yang, Z.M. (2009a), "Fracture assessment of damaged square hollow section (SHS) K-joint using BS7910: 2005", *Eng. Fract. Mech.*, **76**(9), 1303-1319.
- Lie, S.T. and Yang, Z.M. (2009b), "Safety assessment procedure for a cracked square hollow section (SHS) Y-joint", *Adv. Struct. Eng.*, **12**(3), 359-372.
- Lie, S.T., Yang, Z.M. and Gho, W.M. (2009b), "Validation of BS7910:2005 Failure assessment diagrams for cracked square hollow section T-, Y- and K-joints", *Int. J. Press. Vessels Piping*, **86**(5), 335-344.
- Liu, G.J., Zhong, B.L., Tian, X.J., Chen, P.F. and Mu, W.L. (2016), "Numerical analysis on the HSS and SIF of multi-planar DX-joint welds for offshore platforms", *Ocean Eng.*, **127**, 258-268.
- Lu, L.H., de Winkel, G.D., Yu, Y. and Wardenier, J. (1994), "Deformation limit for the ultimate strength of hollow section joints", *Proceedings of the 6th International Symposium on Tubular Structures*, Melbourne, Australia, December, pp. 341-348.
- Mashiri, F.R. and Zhao, X.L. (2010), "Square hollow section (SHS) T-joints with concrete-filled chords subjected to in-plane fatigue loading in the brace", *Thin-Wall. Struct.*, **48**(2), 150-158.
- National Standard of the People's Republic of China (2007), Metallic materials-Charpy pendulum impact test method (GB/T 229-2007).
- Qian, X.D. and Li, Y. (2013), "A compliance-based approach to measure fracture resistance curve for surface cracked steel plates", *Int. J. Fract.*, **182**(1), 1-19.
- Qian, X.D., Zhang, Y. and Choo, Y.S. (2013), "A load-deformation formulation with fracture representation based on the J-R curve for tubular joints", *Eng. Fail. Anal.*, **33**, 347-366.
- Shao, Y.B. (2005), "Fatigue behaviour of uniplanar tubular K-joints under axial and in-plane bending loads", Ph.D. Thesis; School of Civil and Environmental Engineering, Nanyang Technological University, Singapore.
- Shao, Y.B. (2007), "Geometrical effect on the stress distribution along weld toe for tubular T- and K-joints under axial loading", *J. Constr. Steel Res.*, **63**(9), 1351-1360.
- Shao, Y.B. and Cao, Z.B. (2005), "Experimental and numerical analysis of fatigue behaviour for tubular K-joints", *Struct. Mech.*, **19**(6), 639-652.
- Shen, W. and Choo, Y.S. (2012), "Stress intensity factor for a tubular T-joint with grouted chord", *Eng. Struct.*, **35**, 37-47.
- Talei-Faz, B., Brennan, F.P. and Dover, W.D. (2004), "Residual static strength of high strength steel cracked tubular joints", *Marine Struct.*, **17**(3), 291-309.
- Thandavamoorthy, T.S. (2004), "Reserve capacity of fatigue damaged internally ring stiffened tubular joints", *Steel Compos. Struct., Int. J.*, **4**(2), 149-167.
- Wardenier, J., Kurobane, Y., Packer, J.A., Van der Vegte, G.J. and Zhao, X.L. (2008), *Design guide for circular hollow section (CHS) joints under predominantly static loading*; Comité International pour le Développement et l'étude de la Construction Tubulaire (CIDECT), Germany.
- Yagi, K., Tanaka, S., Kawahara, T., Nihei, K., Okada, H. and Osawa, N. (2017), "Evaluation of crack propagation behaviors in a T-shaped tubular joint employing tetrahedral FE modeling", *Int. J. Fatigue*, **96**, 270-282.
- Yang, J.F., Yang, C., Su, M.Z. and Lian, M. (2016), "Stress concentration factors test of reinforced concrete-filled tubular Y-joints under in-plane bending", *Steel Compos. Struct., Int. J.*, **22**(1), 203-216.
- Zerbst, U., Heerens, J. and Schwalbe, K.H. (2002), "The fracture behaviour of a welded tubular joint—an ESIS TC1.3 round robin on failure assessment methods. Part I: experimental data base and brief summary of the results", *Eng. Fract. Mech.*, **69**(10), 1093-1110.

Zhang, Y. and Qian, X.D. (2013), "An eta approach to evaluate the elastic-plastic energy release rate for weld-toe cracks in tubular K-joints", *Eng. Struct.*, **51**, 88-98.

BU